TÜBİTAK

Turkish Journal of Earth Sciences

Volume 34 | Number 4 Article 5

5-26-2025

Integrated geochemical, geoelectrical, and UAV-based methods for analyzing the Güzelyalı landslide (Çanakkale, Türkiye)

OYA ERENOĞLU

EMİN ULUGERGERLİ

R. CÜNEYT ERENOĞLU

ABDULLAH AKBAŞ

AHMET EVREN ERGİNAL

Recommended Citation

ERENOĞLU, O, ULUGERGERLİ, E, ERENOĞLU, R, AKBAŞ, A, & ERGİNAL, A. E (2025). Integrated geochemical, geoelectrical, and UAV-based methods for analyzing the Güzelyalı landslide (Çanakkale, Türkiye). *Turkish Journal of Earth Sciences 34* (4): 548-561. https://doi.org/10.55730/1300-0985.1974

TÜBİTAK

Turkish Journal of Earth Sciences

http://journals.tubitak.gov.tr/earth/

Research Article

Turkish J Earth Sci
(2025) 34: 548-561

doi:10.55730/1300-0985.1974

Integrated geochemical, geoelectrical, and UAV-based methods for analyzing the Güzelyalı landslide (Çanakkale, Türkiye)

Oya ERENOĞLU[1,*], E. Uğur ULUGERGERLİ[2], R. Cüneyt ERENOĞLU[3], Abdullah AKBAŞ[4], A. Evren ERGİNAL[1]

[1]Department of Geography Education, Faculty of Education, Çanakkale Onsekiz Mart University, Çanakkale, Turkiye
[2]Department of Geophysical Engineering, Faculty of Engineering, Çanakkale Onsekiz Mart University, Çanakkale, Turkiye
[3]Department of Geomatics Engineering, Faculty of Engineering, Çanakkale Onsekiz Mart University, Çanakkale, Turkiye
[4]Department of Geography, Faculty of Letters, Bursa Uludağ University, Bursa, Turkiye

Received: 22.06.2024 • **Accepted/Published Online:** 03.03.2025 • **Final Version:** 26.05.2025

Abstract: The number of reactivations increased in the Güzelyalı-Erenköy landslide area after 2013 in Çanakkale, Türkiye, where historical landslide activity has been recorded since 1875. This area is home to numerous summer residences and experiences ongoing slow-moving landslide activity along a 400-m-long slope, extending from the heavily trafficked Çanakkale-İzmir highway to the coastline. In this study, the nature of the reactivations was evaluated by considering the conditioning and triggering factors that contributed to the landslide. The evaluation was based on geochemical analyses, field observations, geoelectric measurements, and unmanned aerial vehicle (UAV) data. The results revealed that the sliding occurred along a moist slip surface, rich in various clay minerals such as illite, montmorillonite, and vermiculite, at a depth of approximately 4.5 m, as determined by ERT (Electrical Resistivity Tomography). Vertical movements within the landslide area, including rises and subsidences, accounted for changes of up to 0.1 m between 2013 and 2023. Chemical Index of Weathering (CIW), Chemical Index of Alteration (CIA), and Plagioclase Index of Alteration (PIA) calculations obtained from the X-ray fluorescence (XRF) spectroscopy analysis indicate that the sliding surface is subjected to strong weathering, and these values are compatible with the X-Ray diffraction (XRD) data.

Key words: Güzelyalı landslide, UAV monitoring, geoelectrical slip detection, landslide reactivation

1. Introduction

Besides the slope and subsurface geometry of the sliding surface, the presence of the clayey layer on the sliding surface has a facilitating effect in the development of landslides (Morgenstern and Tchalenko, 1967; Gillott, 1987; Shuzui, 2001; Wen and Aydin, 2003). The slip surface can be fault planes (Tibaldi et al., 1995; Hart et al., 2012), subhorizontal planes of joint sets (Ekinci et al., 2013), and bedding surface of fold limbs (Wang et al., 2003; Chang et al., 2005; Tsou et al., 2011). This plane of structural weakness allows precipitation and snowmelt waters to penetrate significant depths and the slip surface is covered with a clayey layer due to the weathering over time. Claying is visible evidence of intense weathering at the sliding surface, and the increase in water content, decrease in permeability and increased clay formation constitute the preliminary cause of many landslides developing along weak zones (Skempton and Petley, 1967; Koor et al., 2000). The clay unit that makes up the slip surface can be a combination of multiple types in some cases, so the movement can be triggered due to a interaction of different clay types (Erginal et al., 2009). For example, smectite, kaolinite and illite type clays detected on tuff bearing units interbedded with lignite in an open pit excavation area in Türkiye (Bayhan et al., 1993) gave rise to serious rotational landslides along pre-existing fault planes (Erginal et al., 2008).

Especially in settlements developed on a clay-rich geological sequence prone to landslides and slope failures cause significant deformations. Therefore, it is very important to know the clay types of the critical slip planes where the landslide develops and the subsurface geometry of the clay-covered slip plane before stability analysis and remedial works. Geophysical methods provide very concrete data in this respect in terms of determining the location and geometry of the deep sliding surface based on the electrical resistivity differences from the surface to the deep (Hack, 2000; Jongmans and Garambois, 2007). One of the most used in-situ methods in determining the sliding surface and clayey and water-rich units in landslide surveys is the electrical resistivity tomography (ERT) technique, which is highly preferred in shallow geophysical studies (Ekinci et al., 2013; Perrone et al., 2014). ERT with a wide range of investigation depths is the primary geophysical

* Correspondence: o_turkdonmez@comu.edu.tr

application to investigate the lateral and vertical variations of sliding material in many areas that show different degrees of landslide slope angles (Griffiths and Barker, 1993; de Bari et al., 2011). In general, the ERT anomalies in landslides could result from the substantial electrical conductivity contrast between the bedrock and the sliding body (Havevith et al., 2000; Batayneh and Al-Diabat, 2002), different geological units formed as juxtaposition materials (Bitchler et al., 2004), electrical contrasts within the sliding body which moves with the clayey material and the more stable geological structures (Schmutz et al., 2000; Bekler et al., 2011; Reynolds, 2011).

In addition to knowing and displaying the geochemical composition and nature of the deep slip surface material, precise aerial imaging is of great importance as well. Unmanned aerial vehicles, which are also an important data collection source for geographic information systems, have become a new technology used for mapping landslides. Compared to traditional technologies, faster, more effective, economical and highly accurate results are offered (Booth et al., 2020). Recently, there have been many studies using aerial images collected by UAV equipped with RGB cameras to map, model and/or evaluate in detail the surface effects and kinematics of landslides (Niethammer et al., 2012; Stumpf et al., 2013; Lucieer et al., 2014; James et al., 2017; Rossi et al., 2018). According to Giordan et al. (2018), Gomez and Purdie (2016), and Kucharczyk and Hugenholtz (2021), UAVs, highly detailed 2D and 3D products (orthophotos, digital surface models, etc.) were produced in semireal time.

In the Biga Peninsula where the research area is located, landslides happen in very different geological units, such as Miocene formations containing thick clayey units (Erginal et al., 2009) and andesites that are completely weathered to and covered with a weathering mantle (Ekinci et al., 2013). Landslide activity in an ancient landslide complex around the Erenköy-Güzelyalı area with an area of around 3.75 km^2 has been known since 1875 (Perinçek, 2018) where a considerable population lives at present. This study focuses on an active landslide area located approximately 10 km south of Çanakkale, investigated through geochemical analysis of the sliding surface material, subsurface imaging using ERT, and geomorphological assessment via UAV.

2. Materials and methods

2.1. Location and environmental settings

The Güzelyalı landslide area, situated 14 km south of the coastal city of Çanakkale in northwest Türkiye (Figure 1), occurred within the Çanakkale Formation, which

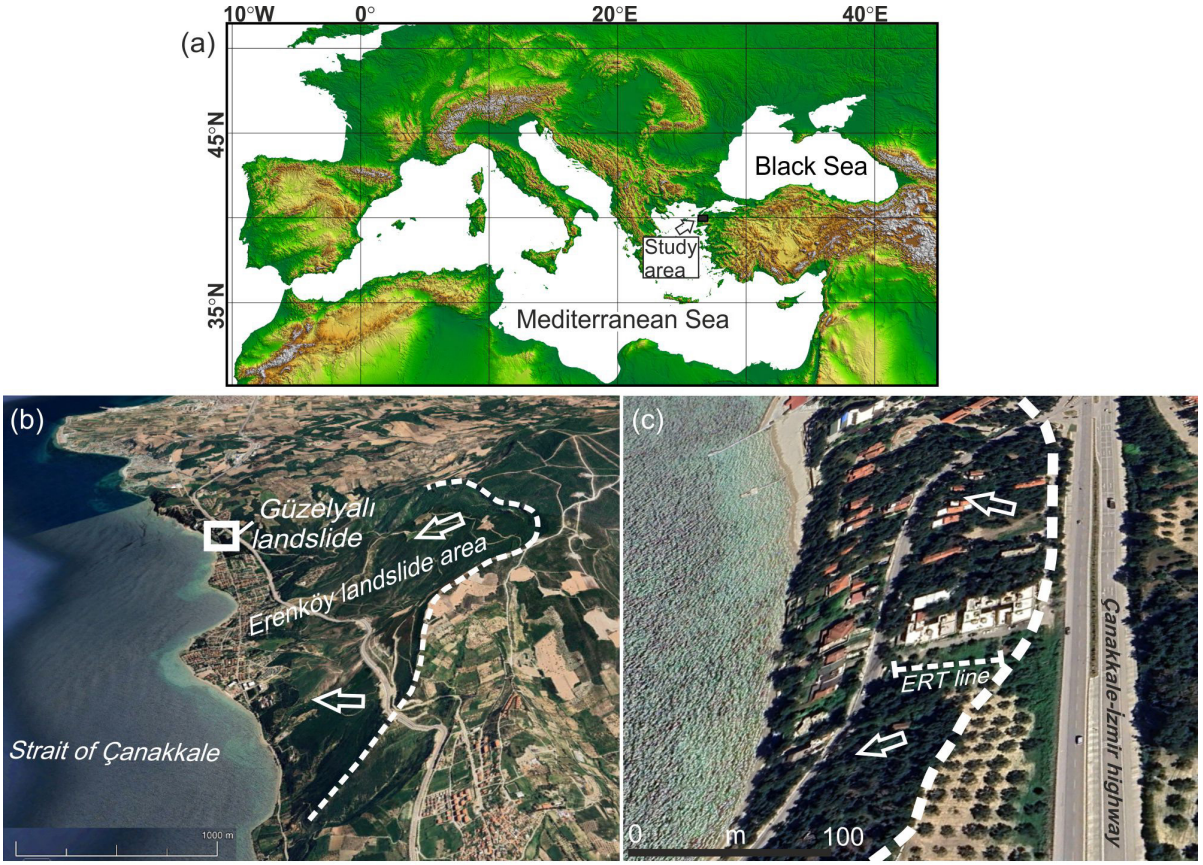

Figure 1. Location map of the study area (a) and Google Earth satellite images showing the landslide area and settlement zones (b–c).

comprises conglomerate, sandstone, mudstone, siltstone, marl, calcarenite, and oolitic limestone (Şentürk and Karaköse, 1987). In this region, the surface outcrops are predominantly composed of units from the Güzelyalı Member of the Çanakkale Formation, which are characterized by medium-grained sandstone, along with lesser amounts of mudstone, claystone, and carbonate units in the lower sections (Figure 2). The landslide area is located on the seaward slopes of the Çanakkale-İzmir highway, in an olive grove with a slope of approximately 10°. The area is located close to the Erenköy (İntepe) landslide area, which is known as a historical landslide area and where landslide activity has continued since 1875 (Perinçek, 2018). Perinçek (2018) revealed that the historical landslide activity, triggered by the 1875 Erenköy-Çanakkale Earthquakes, affected a wide area, including the Güzelyalı landslide. In the context of recorded landslide activity between 1875 and 2013 in the Güzelyalı landslide area, a recent mass movement that began in November 2001 and accelerated in January 2004 was followed by reactivations in the spring of 2005, the fall of 2008, the summer of 2011, and February 2023 (Bekler et al., 2016).

According to the 1929-2022 data from the Çanakkale meteorological station, located 12 km away from the study

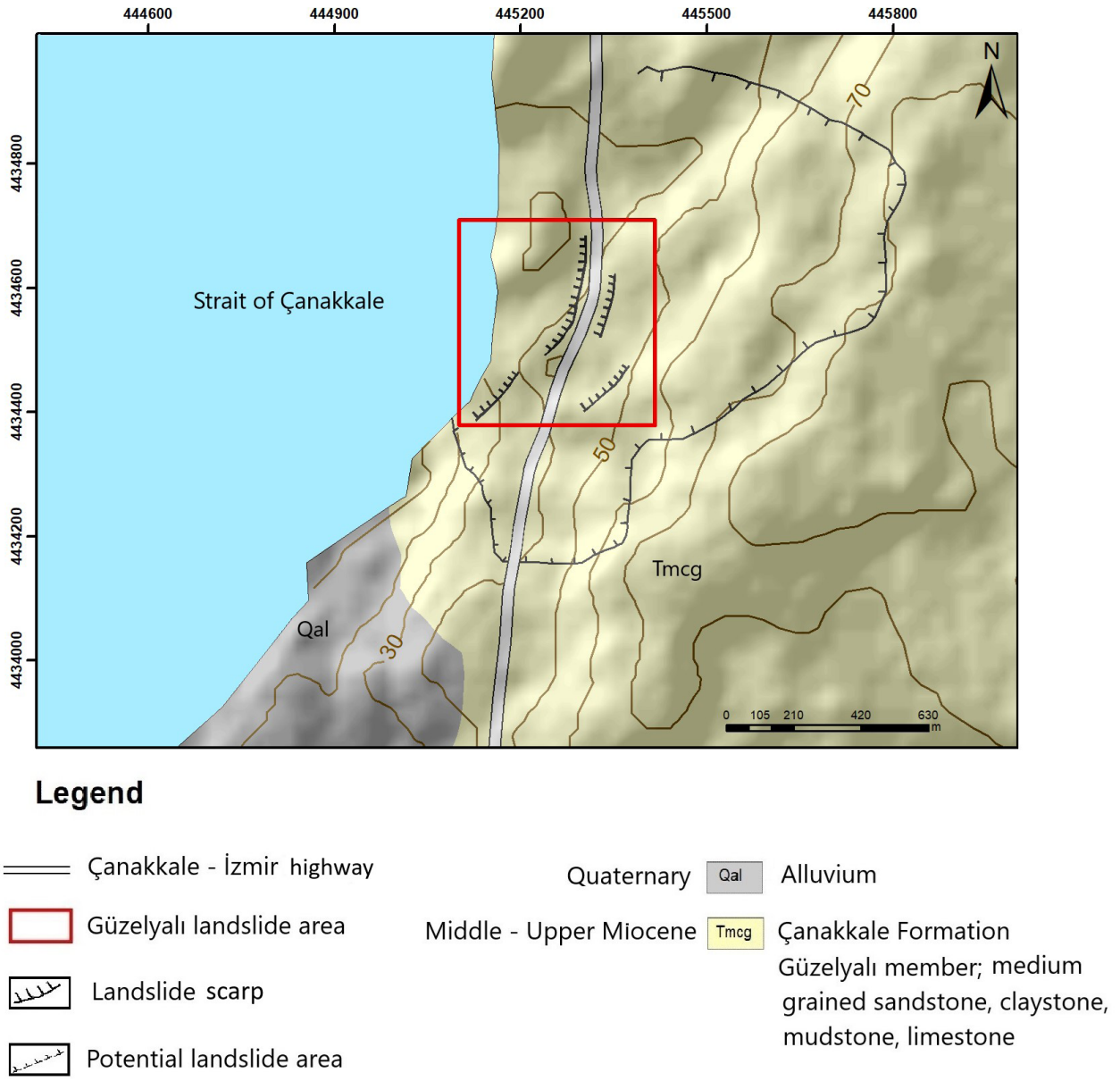

Figure 2. Geological map of the study area.

area, the annual average temperature of the study site is 15 °C, and the annual total precipitation is 630 mm. A significant portion (42%) of the annual total precipitation occurs during the winter months. Summers are quite dry, with evaporation exceeding 200 mm per month during the summer period. According to the Köppen-Geiger climate classification, the region falls under the Mediterranean climate (Csa type), which corresponds to a typical Mediterranean climate (Taşoğlu et al., 2024). Data obtained from 42 years of daily total precipitation measurements recorded at the same station between 1970 and 2022 indicate significant seasonal and annual fluctuations in precipitation patterns. An annual time series analysis reveals that following the last reactivation in 2013, the region experienced a notably rainy period in 2021 (Mucan and Yıldırım, 2023).

2.2. Sampling and geochemical analyses

Field studies were carried out on a slope where landslide activity was observed in 2013 and slope instability is observed today. Sixteen slip surface samples were taken from the upper section of the landslide area, specifically from the main slip plane along the slope of approximately 20°, where the surface fracture was observed. Samples of 10 g were separated from the samples taken, these samples were dried in an oven at 50° for 24 h, and were crushed to powder fineness. The mineral compositions and especially the clay types of these samples were determined by X-ray diffraction (XRD) method. Analyzes were carried out at Çanakkale Onsekiz Mart University Science and Technology Application and Research Center (ÇOBİLTUM).

XRF analyses were performed in Bureau Veritas (Canada) laboratory to determine major oxides in samples taken along the observed slip surface. By using these data, the Chemical Index of Alteration (CIA; Nesbitt and Young, 1982), Plagioclase Index of Alteration (PIA; Fedo et al., 1995), and Chemical Index of Weathering (CIW; Harnois, 1988) calculations were made to determine the degree of weathering of the samples taken from the slip surface. The index formulas are as follows:

$$CIA = (100)\,[Al2O3/(Al2O3 + CaO + Na2O+K2O)] \quad (1)$$

$$PIA = (100)[(Al2O3 - K2O)/(Al2O3 + CaO + Na2O - K2O)] \quad (2)$$

$$CIW = (100)[Al2O3/(Al2O3 + CaO + Na2O)] \quad (3)$$

2.3. Precipitation analyses

Data analyses of satellite and gauge precipitation were conducted to understand the role of precipitation in landslide occurrences. Satellite precipitation data was obtained from IMERG (Huffman et al., 2014). Additionally, precipitation anomaly maps for January and February, during which the landslide occurred, were created to illustrate the precipitation distribution across the study area. Daily precipitation data from the Çanakkale meteorological station (ICAO code: 17112) was sourced from the Turkish Meteorological Service for the period between 1960 and 2016. The daily precipitation anomaly was calculated by subtracting the daily precipitation from the long-term average and dividing it by its standard deviation. Finally, a box plot was generated to visualize the temporal distribution of precipitation anomalies.

2.4. Electrical resistivity tomography (ERT) measurements

Based on the electrical contrast from the subsurface to the deep (Hack, 2000; Jongmans and Garambois, 2007), ERT was used to identify the subsurface nature of the slip surface as it allows taking measurements sensitive to vertical and lateral changes in the underground (Batayneh and Diabat, 2001; Göktürkler et al., 2008; de Bari et al., 2011). Figure 3 illustrates the 4-electrode array for the ERT study (Griffiths and Barker, 1993). It is simply the combination of vertical electrical soundings (VES) conducted for n levels by increasing the interval of electrodes (Ertekin and Ulugergerli, 2022). In the study, the data were gathered using the ARES multi-electrode system. Two-dimensional (2D) inversion of the ERT data was done with the well-known software RES2DINV (Loke and Barker, 1996).

2.5. UAV assisted data acquisition

A part of the dataset used to model the Güzelyalı Landslide was obtained by applying image processing techniques to aerial images collected by UAVs (Figure 4).

2.5.1. Structure from motion for high-resolution photogrammetry

The basic structure from motion (SfM) algorithm was used to produce high-resolution photogrammetric result products such as orthophotos, digital surface, and elevation models after the baseline UAV data were collected. Structure from motion is a computer vision method used that relies on processing multiple stereo images with at least 70% side and frontal overlap to model the 3D surface of objects (Ullman, 1976, 1983). Especially with the improvements in the performance of processors and the development of high-capacity UAVs, the use of SfM has also increased significantly in various scientific fields and landslide studies in the last decade (Westoby et al., 2012; Fonstad et al., 2013; Rossi et al., 2018; Türk, 2018; Valkaniotis et al., 2018; Zárate et al., 2021). As a result of the SfM process, point clouds with X, Y, Z, and RGB spectrum information attached to each point are obtained as photogrammetric products. By processing point clouds, derived photogrammetric products such as digital surface models, orthoimages, and digital elevation models are provided (Rossi et al., 2018; Türk, 2018).

2.5.2. UAV surveying flights

In this study, rotor wings of UAVs developed and widely used for geological and geomorphological research within

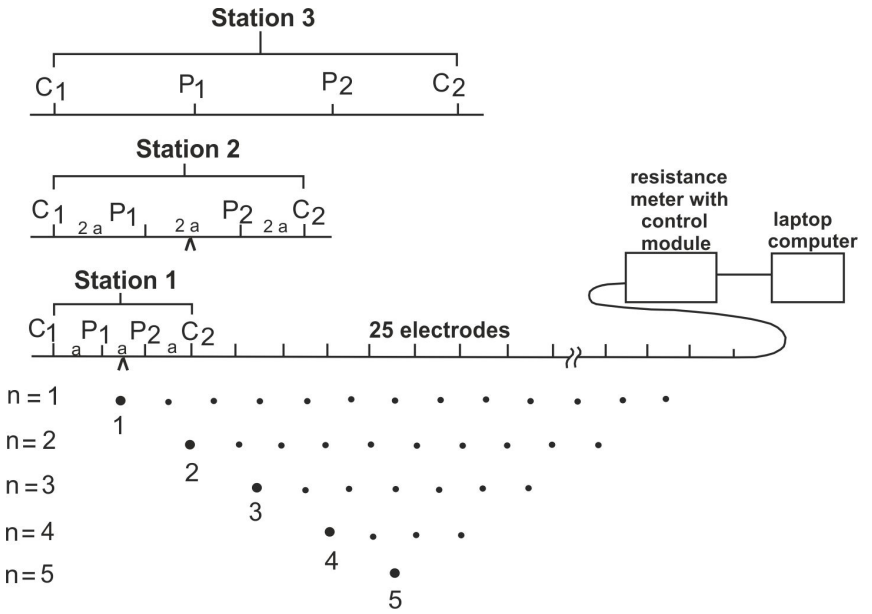

Figure 3. Tomography measurement system; station-1 with interval of a, station-2 with interval of 2a, station-3 with interval of 3a, and so on (Griffiths and Barker, 1993).

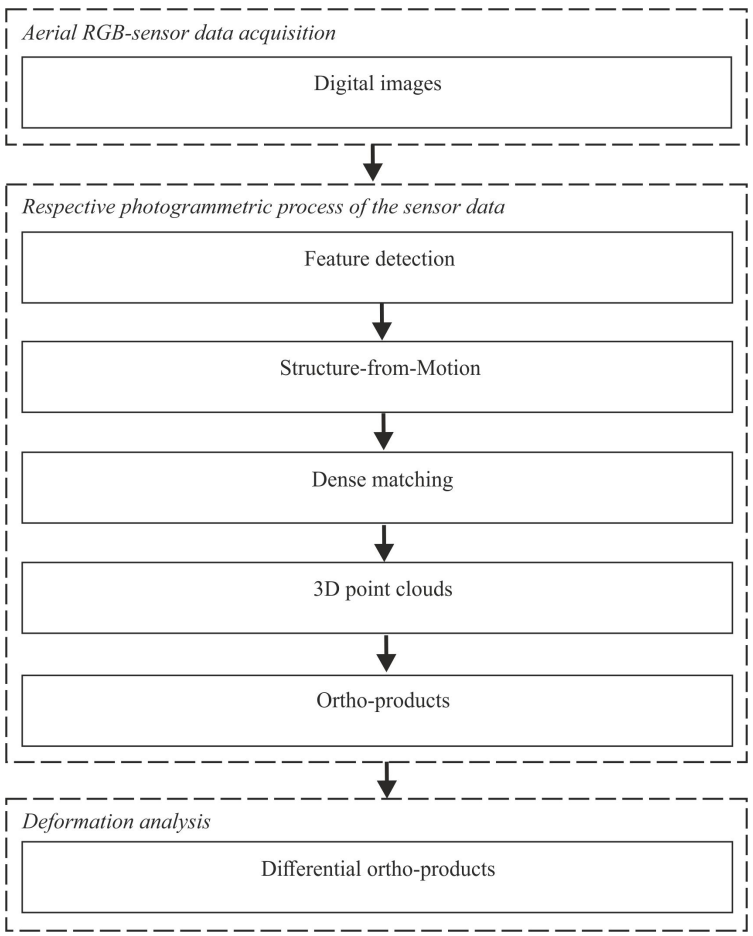

Figure 4. Flowchart of UAV data acquisition, processing, landslide identification, and monitoring.

the scope of modeling the surface topography were used (Fonstad et al., 2013; Micheletti et al., 2015). For this purpose, a DJI Phantom 4 Pro plus rotor wings UAV and ready integrated camera were used in March 2013 and February 2023. The RGB sensor of the integrated camera is 1″ CMOS. Its resolution and focal length are 20 Mpx (image resolution 5472 pixels and 3648 pixels) and 8.8 mm (24 mm in 35 mm format equivalent), respectively.

For georeferencing an image, 6 Ground Control Points (GCP) were placed in the landslide area before the flight. Accurate and precisely positioned ground control points (GCPs) enable successful positioning of photos collected from any UAV platform. The UAV was used together with the SATLAB GNSS and the RTK corrections were ±0.01 m horizontally and ±0.03 m vertically. Flight planning is designed with 100 predefined waypoints in Google KML format. The distance between 20 parallel adjacent flight lines is planned to be approximately equal to strip and across-strip overlaps of about 80% and 60%, respectively. All photos were self-calibrated by the software. Orthogonal photographs were taken during flight at an altitude of 30 m from the starting point in order to obtain appropriate image coverage and a high level of detail of the study area. Each photo covers a different size photo depending on flight altitude. The flight mission took about 20 min to complete. A series of images were taken to cover the entire study area.

After the flight, aerial photographs taken from the landslide area were downloaded, checked, and stored as 16-bit TIFFs. Before the image processing stage, the internal orientation was successfully defined in the camera calibration stage mentioned earlier. Image correlation was used as a relative orientation to transfer anchor points between images. The connection points were used to align all the images taken during the UAV flight under the same conditions. A digital surface model was created by evaluating 100 digital image sets obtained during the UAV flight in SfM (Agisoft 2016) based Agisoft Photoscan Professional Edition software.

3. Results and discussion

3.1. Geological and geomorphological characteristics

On the Çanakkale-İzmir highway, where the landslide took place, yellow-beige colored medium-grained, unconsolidated, massive-looking loose sandstones are common, while hardened, well-cemented sandstone layers (N70W/19NE) with thicknesses varying between 1–8 cm are also observed between loose sandy units. In areas with loose sandy material, abundant cracked surfaces are formed, and in the lower part of this level there are gray mudstones containing thin claystone bands. White claystone nodules, which are abundant in gray mudstones at the lower levels of the Güzelyalı member (Atabey et al., 2004; Yiğitbaş et al., 2005; Yiğitbaş, 2016) in the region, must have also been effective in the formation of landslides due to their water holding properties. However, it has been reported that many factors were effective in the constant occurrence and uncontrollability of landslides in the field since 1875; Çanakkale-İzmir Highway passing through clayey units under heavy traffic load, engineering errors in road construction, increasing the slope of the roadside, inexperience of workers, burnt forest in the region and earthquakes greater than 3 in the region (Perinçek, 2018).

Even though the major reactivation occurred in February 2013, previous landslide activities were recorded in 2000, 2004, 2008, and 2011 (Tunusluoğlu and Karaca, 2016; Tunusluoğlu, 2023). Tunusluoğlu (2023) reported that the landslides affecting approximately two-thirds of the 45 summer houses at the entrance of Güzelyalı village, which occurred initially in November 2001 and were repeated in January 2004, spring 2005, and autumn 2008, coincided with rainy periods and caused separations in adjacent buildings, vertical displacements of 60 to 80 cm at garage entrances relative to road level, backward tilting of approximately 7° in some structures at the toe region of the sliding mass, and settlements of 15 to 20 cm in building foundations. The last great reactivation in the Güzelyalı landslide area occurred in early February 2013. This landslidecaused swelling, rupture, and separation on the highway in the settlement area in Güzelyalı, while creating deformation in nearly 20 luxury villa-type residences. Among the main damages determined are lateral tilting, warping, swelling, and tilting of the garden walls forward (to the sea), the development of horizontal, vertical, and semihorizontal cracks in the walls of the houses, swelling and lowering type deformations caused by the pressure increase in the residential floors and gardens. The backward tilting of buildings that exceeds 10° in many buildings explains that the motion takes place along a rotational slip surface.

The devastating landslide activity in 2013 is related to the anomaly in precipitation after 2012. Figure 5a presents the daily precipitation anomalies between 1960 and 2016, along with the precipitation anomaly maps for January and February. The landslide that occurred in February 2013 can be attributed to these precipitation anomalies. At the end of 2012, the daily precipitation anomaly reached a significantly high positive value for the analyzed period, and this positive anomaly trend persisted through the first and second months of 2013 (Figure 5b). The spatial distribution of monthly precipitation indicates that the study area experienced positive precipitation anomalies. This finding underscores the critical role of antecedent moisture (precipitation) in the development mechanism of the Güzelyalı landslide, surpassing the influence of a single-event triggering mechanism that typically induces landslides over shorter periods.

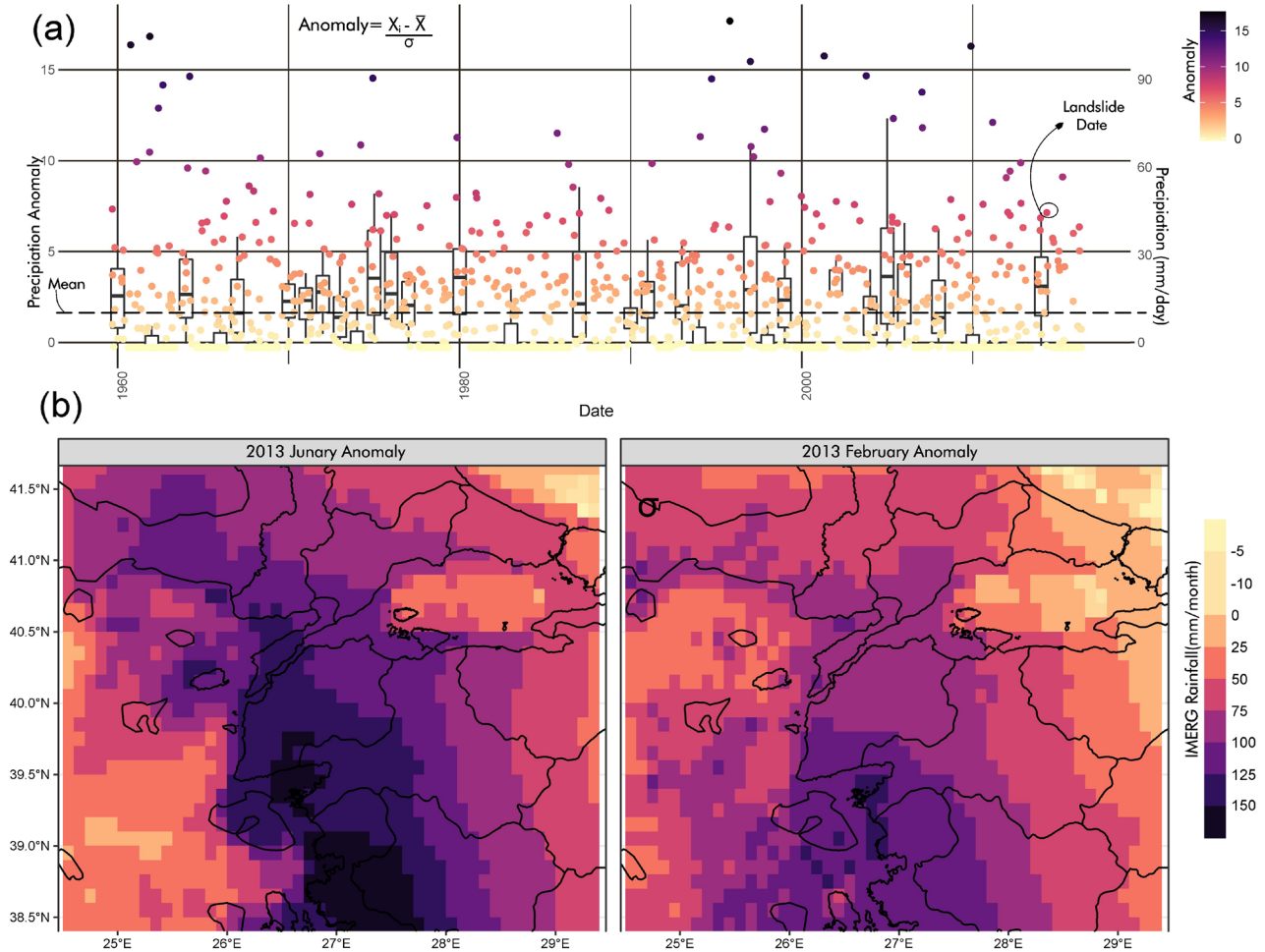

Figure 5. (a) Daily precipitation anomaly plot and (b) January and February precipitation anomaly maps.

In the observations made in March and April of 2021, 2022, and 2023, it was determined that swelling and separation had started on the road, similar to 2013. It was observed that the concrete patches on the floors and walls that were deformed during the 2013 reactivation were reopened, and deformation developed along roughly the same slip plane. The highway was patched with wet asphalt to cover the cracks in late winter 2023. Openings between the water gutters on the side of the highway and the pavement, slopes of garden walls exceeding 10° downhill, and pressure-related swellings are observed almost everywhere along the highway. Traces of the deformation on the highway in 2013 and the reactivation that started in 2021 and 2022 are shown in Figure 6.

There is tilting of almost all red pine trees on the approximately 400 m long slope extending from the Çanakkale-İzmir highway to the coastline. In the Güzelyalı landslide area, one of the most typical signs of the landslide on the surface is the 30° inclination of the red pine trees down the slope toward the sea. In particular, the seismic activity created in the landslide area by the Gülpınar-Ayvacık earthquake (Özden et al., 2018) and Midilli (Kiratzi, 2018) earthquakes and the intense earthquake storm that followed must have had a significant impact on the slope instability in the field since main reactivation in 2013. On the other hand, the devastating 1953 earthquake caused by the Yenice-Gönen Fault (Herece, 1985; Tokay and Dirik, 2004; Kürçer, 2006; Kürçer et al., 2008) should have an important place among the increasing reactivations in the last 70 years.

3.2. Chemical properties of slip surface

The mineral content and major oxide analysis results of 16 samples taken from the slip surface extending at right angles to the ERT measurement line are shown in Figure 1c. The determined major oxide ratios are shown in Table 1. Accordingly, the order of weight according to the average values of the major oxides in the samples are as follows; SiO_2 (55.60%) > Al_2O_3 (9.79%) > CaO (7.44%)

Table 1. Major oxides in slip surface samples based on XRF analysis results (%).

	Major oxides											
Sample	SiO_2	Al_2O_3	Fe_2O_3	MgO	CaO	Na_2O	K_2O	TiO_2	P_2O_5	MnO	Cr_2O_3	LOI
S1	57.42	9.86	3.53	2.27	7.93	1.07	2.06	0.50	0.13	0.09	0.023	14.9
S2	58.38	9.77	3.44	2.50	7.60	1.08	2.05	0.51	0.12	0.09	0.025	14.3
S3	57.33	9.95	3.49	2.74	7.81	1.07	2.05	0.50	0.10	0.10	0.027	14.7
S4	59.24	9.86	3.52	2.83	6.96	1.15	2.06	0.50	0.10	0.10	0.027	13.5
S5	58.84	10.36	3.73	2.68	7.15	1.07	2.14	0.50	0.08	0.10	0.026	13.2
S6	58.14	9.76	3.78	3.26	6.96	1.11	1.97	0.49	0.09	0.10	0.035	14.1
S7	59.59	9.29	3.31	3.20	6.66	1.21	1.92	0.48	0.09	0.10	0.032	14.0
S8	59.27	9.71	3.47	3.05	7.25	1.25	1.95	0.50	0.09	0.10	0.027	13.2
S9	59.68	9.79	3.28	3.25	6.91	1.29	2.00	0.51	0.09	0.10	0.026	12.9
S10	59.57	9.63	3.35	3.01	7.17	1.24	2.02	0.49	0.09	0.10	0.025	13.1
S11	59.93	9.71	3.23	3.05	7.01	1.25	2.01	0.50	0.10	0.09	0.023	12.9
S12	58.14	9.69	3.41	3.02	7.55	1.19	2.03	0.50	0.09	0.09	0.025	14.1
S13	58.80	9.83	3.24	2.89	7.51	1.18	2.06	0.50	0.10	0.10	0.024	13.6
S14	58.09	9.73	3.33	2.80	7.80	1.11	2.04	0.50	0.11	0.09	0.022	14.2
S15	58.34	9.92	3.35	2.48	7.85	1.12	2.13	0.51	0.10	0.09	0.025	13.9
S16	55.60	9.89	3.47	2.85	9.06	1.09	2.04	0.51	0.11	0.09	0.023	15.1
Average	**58.52**	**9.79**	**3.43**	**2.86**	**7.44**	**1.15**	**2.03**	**0.5**	**0.09**	**0.09**	**0.02**	**13.85**

> Fe_2O_3 (3.43%) > MgO (2.86%) > K_2O (2.03%) > Na_2O (1.15%) > TiO_2 (0.5%) > P_2O_5 (0.09%) = MnO (0.09%) > Cr_2O_3 (0.02%).

The weathering index calculations revealed that minimum, maximum, and average values of PIA are 43.61, 50, and 47.46, respectively (Table 2). These values indicate a low degree of silicate weathering (Saikia et al., 2015). The chemical alteration index (CIA) was calculated as 47.96. The chemical weathering index (CIW) was calculated as 53.27. The CIW giving the ratio for the conversion of feldspar to clay (Nesbitt and Young, 1982; Fedo et al., 1995; Maynard et al., 1995) is close to the known mean value (50) for the dissociation in feldspar.

The results of XRD analysis of the same slip surface samples reveal that the dominant mineral is quartz with an average of 44.48% which is followed by illite (19.73%), albite (15.78%), calcite (8.05%), dolomite (7.82%), montmorillonite (3.13%), muscovite (2.33%). The existence of illite and montmorillonite in the samples is important in terms of landslide potential in the field (Table 2). Previous studies on the relationship between clays and landslides have clearly shown that illite and montmorillonite clay minerals have lower shear strength and higher swelling potential, making them more prone to landslides (Ohlmacher, 2000; Yalçın, 2007). Moreover, illite and montmorillonite play a major role in accelerating the argillization process (Song and Song, 2023). It is known that the swelling nature of montmorillonite disrupts soil stability, causing lateral swelling pressure that leads to damage in surrounding structures (Katti et al., 2014), which can be observed as lateral distortion in many structures in the landslide area.

3.3. Subsurface nature of slip surface

When determining the location for the ERT measurement in the Güzelyalı landslide area, the slopes near the highway, which were destroyed during the major reactivation in March 2013, were selected. In order to determine the ERT measurement line for this area, several factors were considered, including the undulating surface structure, distortions in nearby buildings, the forward tilting of house garden walls, and the backward tilting of stone pines along the highway. However, the topography was excluded from the model because the surface gradient was less than 20° and consisted of a slightly undulating topography. Two dimensional (2D) inversion of the ERT data is shown in Figure 7. The RMS error value is very low (1.69%). In Figure 7, warm colors (red to green) indicate displaced units while cold colors (blue) represent clay and

Table 2. XRD analysis results and weathering index values of slip surface samples. Q = quartz; Cal = calcite; Dol = dolomite; Alb = albite; Ver = vermiculite; Mus = muscovite; Crh = chrysotile; Ill = illite; Mon = montmorillonite; Fel = feldspar.

	Minerals										**Weathering indexes**		
Sample	Q	Cal	Dol	Alb	Ver	Mus	Crh	Ill	Mon	Fel	**CIA**	**PIA**	**CIW**
S1	43.9	10.3	-	21.1	-	-	0.2	24.5	-	-	47.13	46.42	52.27
S2	49.1	7.7	3.1	19	-	-	0.1	21	-	-	47.65	47.07	52.95
S3	41.2	8.8	2.8	17	0.8	-	-	29.4	-	-	47.65	47.07	52.84
S4	52.2	6.1	9.5	17	-	-	0.2	14.6	0.3	-	49.22	49.02	54.86
S5	41.4	8.9	3.8	8.5	0.4	-	-	26	-	11	50	50	55.75
S6	31.3	3.7	7.6	8.2	0.3	-	-	-	48.8	-	49.29	49.11	54.73
S7	50.3	7.4	8.1	18	0.3	16	-	-	-	-	48.68	48.35	54.13
S8	53.5	5.7	8.9	23.4	0.4	-	-	8.1	-	-	48.16	47.72	53.32
S9	48.4	4.3	11.8	18.3	-	-	0.2	17	-	-	48.97	48.71	54.41
S10	44.9	7	14.6	12.6	0.7	-	0.2	20	-	-	48.00	47.50	53.38
S11	40.8	7.5	7.7	22.1	0.6	21.3	-	-	-	-	48.59	48.24	54.03
S12	55.2	9	9.1	13.8	0.5	-	-	12	0.4	-	47.36	46.70	52.57
S13	37.5	9	9.2	18.1	-	-	-	20.1	0.3	-	47.76	47.20	53.07
S14	44.6	11.8	8.2	12.7	-	-	-	22.3	0.3	-	47.05	46.32	52.19
S15	39	11.5	9.6	10.4	0.7	-	-	18.7	-	9.8	47.19	46.47	52.51
S16	43.2	10.2	11.2	12.4	0.3	-	-	22.8	-	-	44.79	43.61	49.35
Average	**44.48**	**8.05**	**7.82**	**15.78**	**0.31**	**2.33**	**0.05**	**19.73**	**3.13**	**1.3**	**47.96**	**47.46**	**53.27**

Figure 6. Images showing damage from the 2013 landslide and subsequent reactivation in 2021 and 2022, with their locations marked on the provided aerial photograph.

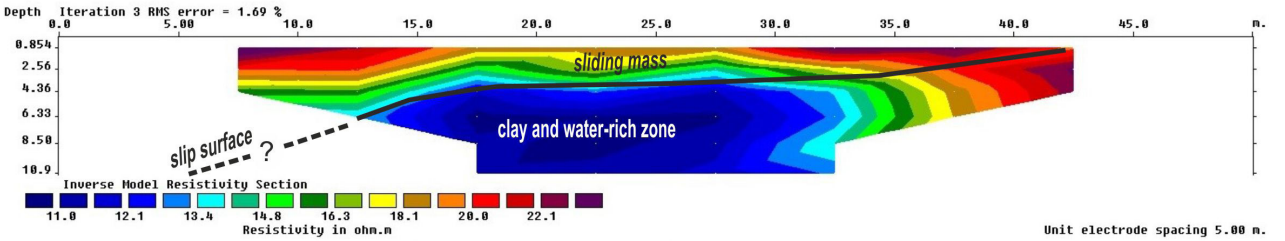

Figure 7. Two dimensional (2D) inversion of the ERT data.

water-bearing units acting as base. Direction of the mass movement is toward 0 m. Movement occurs over the silt unit resides over clay.

Here, it shows the sliding surface with a maximum slope of 10° toward the sea (westwards) from the point where the first electrode was driven, which is 43 m above sea level. The resistivity value, which is a maximum of 22 ohm.m on the surface, varies between 22–13 ohm.m in the sliding mass. The unit, rich in water and clay, determined at a depth of 4.5 m, dives toward the sea with a slope exceeding 30°, starting from the 27th m of the section (17th electrode point). Although the part from the point marked with a question mark in the ERT section to the shoreline cannot be measured, it is clearly seen that the sliding surface marked by a sudden contrast change in resistivity values is rapidly inclining toward the sea. This unit, which is rich in illite (approximately 20%) in the clayey unit of the Güzelyalı member, is saturated with water and is represented by high conductivity and low resistivity down to 11 ohm.m.

Accordingly, the main issue that should be taken into consideration in engineering applications is that the sliding surface in the section extends between 4.5–6 m and dives toward the sea. In the red pine forest on the slope, all deformations such as the tilting of the trees as well as the distortion of the houses (backward tilting) are also related to the nature of the sliding surface.

3.4. Temporal change of vertical deformation

UAS-assisted digital photogrammetry based on Structure from Motion (SfM) algorithms was used to derive a very high spatial resolution DSM and orthophoto mosaic (1 mm). For the digital imagery, 2.2 million point textured mesh of the pile were derived from a 14.1 million point DSM from PhotoScan. Dense surface model and the other submodels obtained from digital imagery are seen in Figure 8. The submodels and final products obtained during the photogrammetric process from aerial photographs captured by the unmanned aerial vehicle, as indicated in Figures 8a–8f, are as follows: (a) Dense surface model obtained, (b) point cloud model, (c) dense cloud model, (d) dense cloud classes model, (e) wireframe model, (f) textured model. To test the UAS image model and RTK/GNSS survey against each other, we used a distance measurement between point clouds or meshes based on the nearest neighbor, i.e. the Euclidean distance. According to the results, the mean and standard deviation between the ground control points surveyed by RTK/GNSS and obtained from UAS image models are 0.017 m and 0.028 m, respectively. It seems quite small given the expected accuracies of the methods employed.

Figure 8g shows the differential model of the Güzelyalı area derived from data acquired between March 2013 and February 2023, revealing vertical surface deformation, including areas of rise and settlement reaching 0.1 m. This period encompasses a landslide reactivation event on July 5, 2016, triggered by winter precipitation. The model accurately depicts surface deformation at specific landslides, validated by comparison with GPS measurements, with differences typically less than 0.1 m. The area incorporates GCP points and a long-term GPS monitoring station. Multitemporal modeling facilitates dynamic monitoring of surface deformation, enabling early landslide identification. On the other hand, the annual rate for deformation analysis is statistically calculated based on a total displacement of 10.5 cm. The observation period spans from March 2013 to February 2023, covering a total duration of 10 years. However, the calculation requires a detailed examination of the time frame on a monthly basis. The total duration, expressed in years, from March 2013 to February 2023, is determined as follows: Considering the specific start and end months, the total observation period comprises 10 full years. Consequently, the annual rate is computed to be approximately 1.06 cm/year and this rate showed the slow movement based on the photogrammetry measurements in studying landslide scarp. As is well known in the literature, slow-moving landslides, such as the Güzelyalı Landslide, can exhibit displacement rates ranging from millimeters to meters per year (Dikbaş et al., 2018; Cascini et al., 2020). Although these slow-moving landslides may appear stable, their often insidious nature can pose significant risks to infrastructure and communities (Highland et al., 2009). Slow-moving

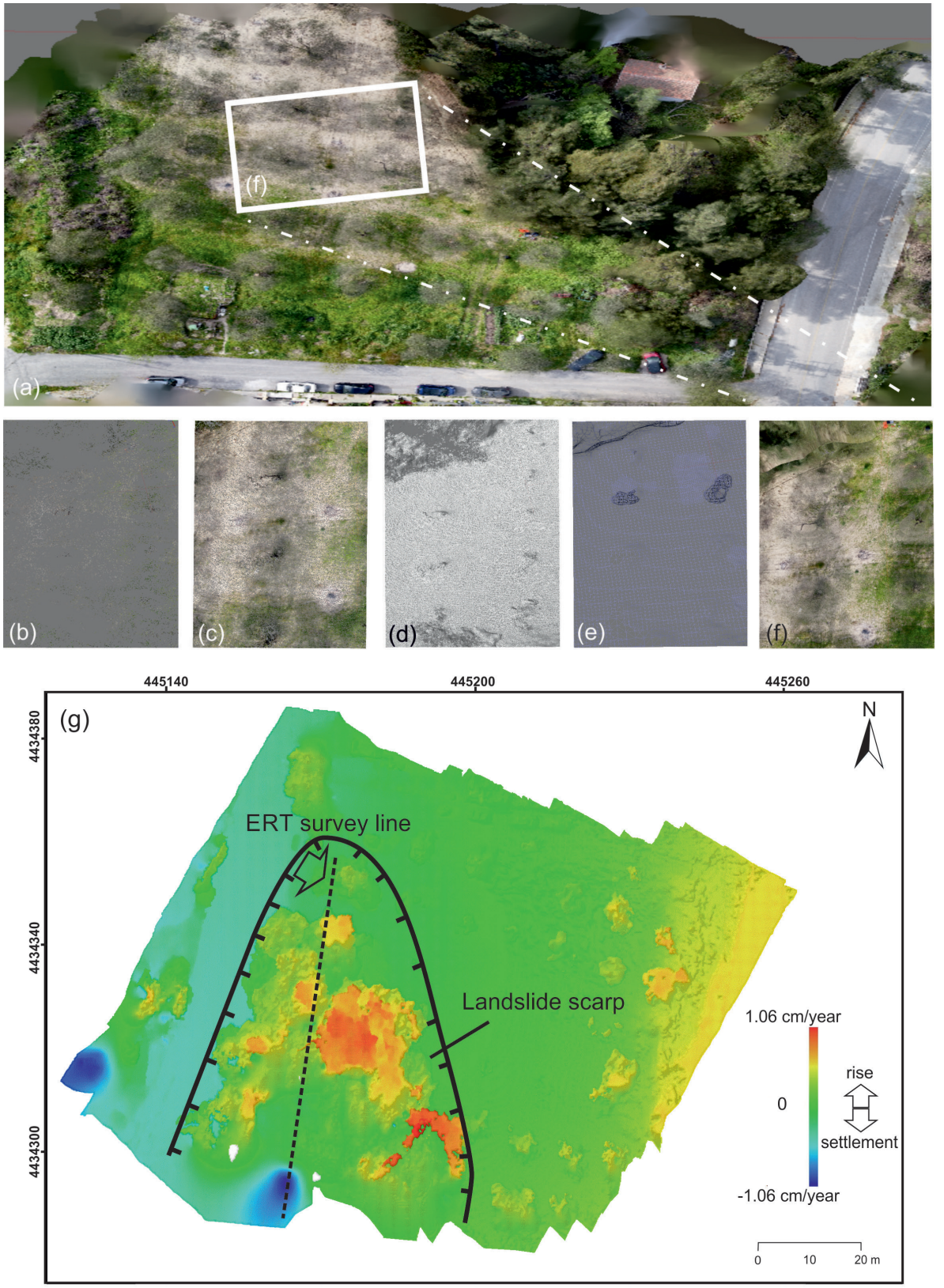

Figure 8. Vertical deformation map of the landslide slope expressed in annual rates, obtained by differentiating digital surface models acquired between March 2013 and February 2023.

landslides, like the Güzelyalı Landslide, can be particularly challenging to detect due to their gradual displacement rates (Cascini et al., 2020). This can lead to a false sense of security, as highlighted by Highland et al. (2009), who emphasize the importance of long-term monitoring for these types of landslides. The Güzelyalı Landslide, a representative example of slow-moving landslides in the region, has been extensively studied (Yılmaz et al., 2015). The findings of these studies corroborate the international literature, which suggests that slow-moving landslides can pose significant hazards, even when displacement rates appear minimal (Dikbaş et al., 2018).

4. Conclusion

In the Güzelyalı landslide area, reactivated in the toe of the historical Erenköy landslide area near the coast of the Strait of Çanakkale, landslide reactivations occurred since 2013. Although the devastating landslide activity in 2013 was related to the precipitation anomaly after 2012, separations along the sliding surface might have occurred in the region due to the effect of the earthquakes in 2008. The strongly weathered and illite-rich slip surface controls the slow development mechanism of the Güzelyalı landslide. The ground ruptures as well as inclinations in trees and deformations in structures due to 2013 and 2023 reactivations follow the same zones along the moist and clayey slip surface at a depth of 4.5 m. Considering possible reactivations in the future, precautions must be taken. Our results show that a combination of UAV-based orthophotos, differential network models, ERT, and geochemical data can be used for flexible and accurate detection and monitoring of landslides over a wide area. By integrating these different data sources and analysis techniques, this study has provided significant insights into the spatial and temporal understanding and monitoring of slope instability in the historical landslide zone of the region.

Acknowledgment

This work was supported by the Scientific Research Coordination Unit of Çanakkale Onsekiz Mart University, project number: SBA-2021-3628. We thank M. İzmirli (Çanakkale Special Provincial Administration) for assisting us in gathering ERT data.

References

Atabey E, Ilgar A, Sakıtaş A (2004). Çanakkale Havzasının Orta-Üst Miyosen Stratigrafisi, Çanakkale, KB Türkiye, MTA Dergisi 128: 79-97 (in Turkish).

Batayneh AT, Al-Diabat AA (2002). Application of a two-dimensional electrical tomography technique for investigating landslides along the Amman–Dead Sea highway, Jordan. Environmental Geology 42 (4): 399-403.

Bayhan E, Şahbaz A, Görmüş S (1993). Clay sedimentology of the sedimentary sequence in open-pit mines in Çan (Çanakkale), Orhaneli and Keles (Bursa). Bulletin of the Mineral Research and Exploration 115: 71–76.

Bekler T, Ekinci YL, Demirci A, Erginal AE, Ertekin C (2011). Characterization of a landslide using seismic refraction, electrical resistivity and hydrometer methods, Adatepe—Çanakkale, NW Turkey. Journal of Environmental & Engineering Geophysics 16 (3): 115-126. https://doi.org/10.2113/jeeg16.3.115

Bekler T, Demirci A, Ekinci YL (2016). Heyelan Alanlarında Mühendislik Jeofiziği Parametreleri ve Değerlendirmeleri: Güzelyalı ve Lapseki Adatepe Örnekleri, s. 27-51. Çanakkale Heyelanları Kitabı, 190 s., Altın Kalem Yayınları (in Turkish).

Cascini L, Crosta GB, Frattini P (2020). Slow-moving landslides and their impact on infrastructure: A case study from the Italian Alps. Landslides, 17 (2): 315-328.

Chang KJ, Taboada A, Chan YC (2005). Geological and morphological study of the Jiufengershan landslide triggered by the Chi-Chi Taiwan earthquake. Geomorphology 71: 293–309. https://doi.org/10.1016/j.geomorph.2005.02.004

de Bari C, Lapenna V, Perrone A, Puglisi C, Sdao F (2011). Digital photogrammetric analysis and electrical resistivity tomography for investigating the Picerno landslide (Basilicata region, southern Italy). Geomorphology: 133 (1-2): 34-46.

Dikbaş AA, Kaya Y, Çalık H (2018). Yavaş Hareketli Heyelanların İnSAR ile Monitöringi: Güzelyalı Heyelanı Örneği. Türkiye Jeoloji Bülteni, 61 (2): 115-128 (in Turkish).

Ekinci YL, Türkeş M, Demirci A, Erginal AE (2013). Shallow and deep-seated regolith slides on deforested slopes in Çanakkale, NW Turkey. Geomorphology 201: 70–79. https://doi.org/10.1016/j.geomorph.2013.06.008

Erginal AE, Türkeş M, Ertek TA, Baba A, Bayrakdar C (2008). A geomorphological investigation of the excavation induced Dundar Landslide, Turkey. Geografiska Annaler Series A: Physical Geography 90 (2): 109-123. https://doi.org/10.1111/j.1468-0459.2008.00159.x

Erginal AE, Öztürk B, Ekinci YL, Demirci A (2009). Investigation of the nature of slip surface using geochemical analyses and 2-D electrical resistivity tomography: a case study from Lapseki area, NW Turkey. Environmental Geology 58 (6): 1167-1175. https://doi.org/10.1007/s00254-008-1594-4

Ertekin C, Ulugergerli EU (2022). Geoelectrical survey over perched aquifers in the northern part of Upper Sakarya River Basin, Türkiye. Journal of Groundwater Science and Engineering 10 (4): 335-352. https://doi.org/10.19637/j.cnki.2305-7068.2022.04.003

Fedo CM, Nesbitt HW, Young GM (1995). Unraveling the effects of potassium metasomatism in sedimentary rocks and paleosols, with implications for paleoweathering conditions and provenance. Geology 23: 92 1 -924. https://doi.org/10.1130/0091-7613(1995)023<0921:UTEOPM>2.3.CO;2

Fonstad MA, Dietrich JT, Courville BC, Jensen JL, Carbonneau PE (2013). Topographic structure from motion: a new development in photogrammetric measurement. Earth Surface Processes and Landforms 38: 421-430. https://doi.org/10.1002/esp.3366

Gillott JE (1987). Clay in Engineering Geology. Elsevier Publication Company, Amsterdam.

Göktürkler G, Balkaya C, Erhan Z (2008). Geophysical investigation of a landslide: The Altındağ landslide site, İzmir (western Turkey). Journal of Applied Geophysics 65: 84–96. https://doi.org/10.1016/j.jappgeo.2008.05.008

Griffiths DH, Barker RD (1993). Two-dimensional resistivity imaging and modelling in areas of complex geology. Journal of Applied Geophysics 29 (3-4): 211-226. https://doi.org/10.1016/0926-9851(93)90005-J

Hack R (2000). Geophysics for slope stability. Surveys in Geophysics 21: 423–448. https://doi.org/10.1023/A:1006797126800

Hart MW, Shaller PJ, Farrand GT (2012). When Landslides Are Misinterpreted as Faults: Case Studies from the Western United States. Environmental & Engineering Geoscience 18 (4): 313–325. https://doi.org/10.2113/gseegeosci.18.4.313

Harnois L (1988). The CIW index: A new chemical index of weathering. Sedimentary Geology 55 (3-4): 319-322. https://doi.org/10.1016/0037-0738(88)90137-6

Havevith HB, Jongmans D, Abdrakhmatov K, Trefois P, Delvaux D et al. (2000). Geophysical investigations of seismically induced surface effects: case study of a landslide in the Suusamyr valley, Kyrgyzstan. Surveys in Geophysics 21 (4): 351-370. https://doi.org/10.1023/A:1006788808145

Highland LM, Bobrowsky P, Godt JW (2009). Recognizing and Assessing Unstable Slopes in Wildland Areas. Surveys in Geophysics, 30 (4): 347-370.

Herece E (1985). The fault trace of 1953 Yenice–Gönen Earthquake and some examples of recent tectonic events in the Biga Peninsula of Northwest Turkey: Penn State University, Ms. S. Thesis 143 s.

Huffman, G, Bolvin D, Braithwaite D, Hsu K, Joyce R et al. (2014). GPM Integrated Multi-Satellite Retrievals for GPM (IMERG) Algorithm Theoretical Basis Document (ATBD) Version 4.4. PPS, NASA/GSFC, 30 pp.

Jongmans D, Garambois S (2007). Geophysical investigation of landslides: a review. Bulletin de la Société Géologique de France 178 (2): 101–112. https://doi.org/10.2113/gssgfbull.178.2.101f

Katti DR, Katti KS, Srinivasamurthy L (2014). Molecular modeling of onset of swelling in expansive clays, Proceeding of the 14th IACMAG, Kyoto, Japan, 22- 25/9/2014.

Kiratzi A (2018). The 12 June 2017 Mw 6.3 Lesvos Island (Aegean Sea) earthquake: Slip model and directivity estimated with finite-fault inversion. Tectonophysics 724–725: 1–10. https://doi.org/10.1016/j.tecto.2018.01.003

Koor NP, Parry S, Yin JH (2000). The shear strength of infilled and slicksided discontinuities of some Hong Kong saprolites. Engineering Geology HK 2000: 187–192.

Kürçer A (2006). Neotectonical features of the vicinity of Yenice–Gönen and palaeoseismology of March 18, 1953 (Mw:7,2) Yenice–Gönen Earthquake Fault, NW Turkey, M.S. Thesis. Çanakkale Onsekiz Mart University, Natural and Applied Sciences Institute, p. 170 (in Turkish with an abstract in English).

Kürçer A, Chatzipetros A, Tutkun SZ, Pavlides S, Ateş Ö et al. (2008). The Yenice–Gönen active fault (NW Turkey): Active tectonics and palaeoseismology. Tectonophysics 453: 263–275. https://doi.org/10.1016/j.tecto.2007.07.010 (in Turkish).

Loke MH, Barker RD (1996). Rapid leastsquares inversion of apparent resistivity pseudosections using a quasi-Newton method. Geophysical Prospecting 44: 131–152. https://doi.org/10.1111/j.1365-2478.1996.tb00142.x

Maynard JB, Sutton SJ, Robb LJ, Ferraz MF, Meyer EM (1995). A paleosol developed on hydrothermally altered granite from the hinterland of the Witwatersrand basin: characteristics of a source of basin fill. Journal of Geology 103: 357-377. https://doi.org/10.1086/629757?journalCode=jg

Micheletti N, Chandler JH, Lane SN (2015). Section 2.2: structure from motion (SfM) photogrammetry. In: Clarke LE, Nield JM (eds) Geomorphological Techniques (Online Edition). British Society for Geomorphology, London, UK.

Morgenstern NR, Tchalenko JS (1967). Microstructural observations on shear zones from slips in natural clays. Proceedings of Geotechnical Conference, Norwegian Geotechnical Society, Oslo 1: 147-152.

Mucan U, Yıldırım M (2023). Çanakkale İlinin Uzun Yıllar İklim Verilerine Bağlı Kuraklık Analizi, ÇOMÜ Ziraat Fakültesi Dergisi 11 (2): 339-350. https://doi.org/10.33202/comuagri.1395101 (in Turkish).

Nesbitt YW, Young GM (1982). Early Proterozoic climates and plate motions inferred from major element chemistry of lutites. Nature 299: 715-717. https://doi.org/10.1038/299715a0

Ohlmacher GC (2000). The Relationship between geology and landslide hazards of Atchison, Kansas, and vicinity, Kansas Geological Survey Bulletin 244 (3): 1–16. https://doi.org/10.17161/cres.v0i244.11833

Özden S, Över S, Poyraz SA, Güneş Y, Pınar A (2018). Tectonic implications of the 2017 Ayvacık (Çanakkale) earthquakes, Biga Peninsula, NW Turkey. Journal of Asian Earth Sciences 154: 125–141. https://doi.org/10.1016/j.jseaes.2017.12.021

Perinçek D (2018). Geological and geomorphological analysis of the ancient Erenkoy and Guzelyali landslides in the Canakkale District, NW Turkey. Geological Bulletin of Turkey 61 (3): 241-267. https://doi.org/10.25288/tjb.458432

Perrone A, Lapenna V, Piscitelli S (2014). Electrical resistivity tomography technique for landslide investigation: A review. Earth-Science Reviews 135: 65–82. https://doi.org/10.1016/j.earscirev.2014.04.002

Reynolds JM (2011). An introduction to applied and environmental geophysics. John Wiley & Sons. ISBN: 978-0-471-48535-3. p.710

Rossi G, Tanteri L, Tofani V, Vannocci P, Moretti S et al. (2018). Multitemporal UAV surveys for landslide mapping and characterization. Landslides 15: 1045–1052. https://doi.org/10.1007/s10346-018-0978-0

Saikia BJ, Goswami SR, Borthakur R, Roy IB, Borah RR (2015). Spectroscopic characterization and quantitative estimation of natural weathering of silicates in sediments of Dikrong River, India. Journal of Modern Physics 6 (11): 1631–1641. https://doi.org/10.4236/jmp.2015.611164

Schmutz M, Albouy Y, Guérin R, Maquaire O, Vassal J et al. (2000). Joint electrical and time domain electromagnetism (TDEM) data inversion applied to the Super Sauze earthflow (France). Surveys in Geophysics 21 (4): 371-390. https://doi.org/10.1023/A:1006741024983

Shuzui H (2001). Process of slip surface development and formation of slip surface clay in landslide in Tertiary volcanic rocks, Japan. Engineering Geology 61: 199–219. https://doi.org/10.1016/S0013-7952(01)00025-4

Skempton AW, Petley DJ (1967). The strength along structural discontinuities in stiff clays. In: Proceedings of Geotechnical Conference, Oslo 2: 29–46

Song Q, Song K (2023). A Review of the Evolution Characteristics and Argillization of Clay Interbeds in Rockslides, Applied Sciences 13: 11646. https://doi.org/10.3390/app132111646

Şentürk K, Karaköse C (1987). Çanakkale Boğazı ve dolayının jeolojisi. MTA Rap. No: 9333. (in Turkish).

Taşoğlu E, Öztürk MZ, Yazıcı Ö (2024). High Resolution Köppen-Geiger Climate Zones of Türkiye, International Journal of Climatology 44 (14): 5248-5265. https://doi.org/10.1002/joc.8635

Tsou CY, Feng ZY, Chigira M (2011). Catastrophic landslide induced by Typhoon Morakot, Shiaolin, Taiwan. Geomorphology 127: 166–178. https://doi.org/10.1016/j.geomorph.2010.12.013

Tibaldi A, Ferrari L, Pasquarè G (1995). Landslides triggered by earthquakes and their relations with faults and mountain slope geometry: an example from Ecuador. Geomorphology 11: 215-226. https://doi.org/10.1016/0169-555X(94)00060-5

Tokay F, Dirik K (2004). The 1953 Yenice–Gönen Earthquake (Mw:7,2) rupture-fault geometry and slip distribution (SW Strand of North Anatolian Fault System-Turkey). In: Chatzipetros, A., Pavlides, S. (Eds.), Proceedings of the 5th International Symposium on Eastern Mediterranean Geology, Thessaloniki, Greece, 657–658.

Tunusluoğlu MC, Karaca Ö (2016). Çanakkale Kenti Güneybatısını (Güzelyalı) Tehdit Eden Kütle Hareketlerinin Jeoteknik Açıdan Değerlendirilmesi ve Kütle Hareketinin Çevresel Etkileri. In: Çanakkale Heyelanları, E.Yiğitbaş (Ed), Altın Kalem, 40-59 (in Turkish).

Tunusluoğlu MC (2023). Engineering Geological Assessment of a Slope Instability: A Case Study in the Guzelyali Region (Canakkale, Turkey). Yerbilimleri 44 (2): 142–165. https://doi.org/10.17824/yerbilimleri.1281981

Türk T (2018). Determination of mass movements in slow-motion landslides by the Cosi-Corr method. Geomatics Natural Hazards and Risk 9: 325–336. https://doi.org/10.1080/19475705.2018.1435564

Ullman S (1976). The interpretation of structure from motion. *Massachusetts Institute* of *Technology*. A*rtificial Intelligence Laboratory*. A.I. Memo 476, Oct. 1976, 1–7. https://doi.org/10.1098/rspb.1979.0006

Ullman S (1983). Computational studies in the interpretation of structure and motion: summary and extension. *Massachusetts Institute* of *Technology*. A*rtificial Intelligence Laboratory*. A.I. Memo 706, March 1983, 1–25

Valkaniotis S, Papathanassiou G, Ganas A (2018). Mapping an earthquake-induced landslide based on UAV imagery; case study of the 2015 Okeanos landslide, Lefkada. Greece Engineering Geology 245: 141–152. https://doi.org/10.1016/j.enggeo.2018.08.010

Wen BP, Aydin A (2003). Microstructural study of a natural slip zone: quantification and deformation history. Engineering Geology 68: 289–317. https://doi.org/10.1016/S0013-7952(02)00234-X

Wang WN, Chigira M, Furuya T (2003). Geological and geomorphological precursors of the Chiu-fen-erh-shan landslide triggered by the Chi-chi earthquake in central Taiwan. Engineering Geology 69: 1 – 13. https://doi.org/10.1016/S0013-7952(02)00244-2

Westoby MJ, Brasington J, Glasser NF, Hambrey MJ, Reynolds JM (2012). Structure-from-motion photogrammetry: a low-cost, effective tool for geoscience applications. Geomorphology 179: 300–314. https://doi.org/10.1016/j.geomorph.2012.08.021

Yalçın, A (2007). The effects of clay on landslides: A case study, Applied Clay Science 38: 77–85. https://doi.org/10.1016/j.clay.2007.01.007

Yılmaz M, Kaya Y, Dikbaş AA (2015). The influence of rainfall intensity on shallow landslide susceptibility in the Güzelyalı region, Turkey. Landslides, 12 (4): 679-692.

Yiğitbaş E, Baba A, Yılmazer İ, Bozcu M, Deniz O et al. (2005). Güzelyalı (Çanakkale) 27J Paftası Kuzeydoğu Kesiminde Heyelan Etüd Raporu, p. 122 (in Turkish).

Yiğitbaş E (2016). Jeolojik - Antropojenik Sebep - Sonuç ilişkileri açısından Çanakkale Heyelanlarına Toplu Bakış. in: Çanakkale Heyelanları, E.Yiğitbaş (Ed), Altın Kalem Yayınları, İzmir, 9-25 (in Turkish).

Zárate BA, Hamdouni RE, Fernández T (2021). GNSS and RPAS integration techniques for studying landslide dynamics: application to the areas of Victoria and Colinas Lojanas, (Loja, Ecuador). Remote Sensing 13: 3496. https://doi.org/10.3390/rs13173496